Stanford Exploration Project, Report 75, November 17, 1997, pages 53–69

Stanford Exploration Project, Report 75, November 17, 1997, pages 53–69

Migration of crosswell seismic data

Lewei Mo[1]

keywords: *velocity, modeling, imaging, diffraction*

ABSTRACT

Crosswell seismic survey has proven to be an effective, high-resolution method of reservoir characterization. However, its application has been mainly confined to transmission traveltime tomography, even though extensions have recently been made to reflection imaging. This paper describes the application of reverse-time wavefield extrapolation coupled with the excitation-time imaging condition to the migration of crosswell seismic common-shot profiles. I have applied fourth-order-in-time, tenth-order-in-space finite differencing to perform the crosswell seismic modeling of the two-way acoustic wave equation. During the migration wavefield backpropagation, I gradually drop the order of finite differencing to the second-order near the recording boundary for the derivative perpendicular to the recording boundary, so that the numerical computation conforms to physical wave phenomena. Modeling and migration are based on the geometry of a true field survey. This method successfully models high frequency crosswell seismic wavefields. Migration of one common-shot profile gives a very clear reflectivity image. Vertical resolution up to a half wavelength and horizontal resolution as governed by the first Fresnel zone width have been realized. At the end, the paper presents some suggestions to facilitate field data migration, which include removal of tube waves and wavefield separation.

INTRODUCTION

Cross-well seismic survey has proven to be an effective, high-resolution method of reservoir characterization because of its high, wide frequency band (Beydoun et al., 1989). Several researchers (McMechan et al., 1987; Harris, 1988; Bregman et al., 1989; Chen et al., 1990; Luo and Schuster, 1991; Lines, 1991) have developed methods of transmission tomography to produce tomographic velocity cross-sections of the subsurface between the two wells. But transmission traveltime tomography uses only the traveltimes of the first arrivals, which represent only a small fraction of the total information contained in the data. Scattered events in seismic sections, such as reflections and diffractions, carry rich lithologic information. Full realization of the

[1]**email:** not available

potential of crosswell seismic data for detailed delineation of the geological structure requires the imaging of these scattered events, which promises resolution in the scale of wavelength. For this purpose, Pratt and Worthington (1988) applied diffraction tomography and Beydoun and Mende (1989) applied ray-Born migration/inversion to crosswell data. Recently, Lazaratos et al. (1991) applied VSP-CDP mapping to crosswell reflection imaging with success. But a more robust method would have to be based on migration that can honor arbitrary velocity structures. This paper describes such a method, reverse-time migration.

In a crosswell seismic survey geometry, the shots and receivers are located in separate wells. Thus crosswell migration is best considered as a problem of prestack common-shot profile migration. A profile consists of the seismograms of one shot and many receivers. Because it is a true physical experiment, processing of profiles is more fundamental than that of other geometries. Methods of prestack profile migration were first presented by Claerbout (1970, 1976). According to his U/D imaging concept, reflectors exist in the earth at places where the onset of the downgoing wave is time-coincident with an upcoming wave. Several authors have since extended Claerbout's theorem of wavefield extrapolation and the imaging condition (Jacobs, 1982; Reshef and Kosloff, 1986; Chang and McMechan, 1986). Chang and McMechan (1986) generalized Claerbout's imaging condition, and stated the excitation-time imaging condition for prestack reverse-time migration, by which each reflector point is imaged at the one-way direct-wave traveltime from the source to the point at which it is excited. Reverse-time profile migration with the excitation-time imaging condition consists of three elements: (1) computation of the imaging condition, that is, computation of the direct wave traveltime from the source point to every image point, (2) extrapolation backward in time of the common-shot profile wavefields from the receivers into the background velocity model by the two-way wave equation finite-difference method, and (3) imaging. Imaging is performed at each step of the wavefield extrapolation process by extracting, from the propagating wavefields, the values at the particular grid points that are excited and thus imaged at that time and adding them as reflectivity into the image plane at the same spatial locations. The locus of all points imaged at one time step corresponds to the direct wave exciting wavefront from the source.

Hu et al. (1988) and Zhu et al. (1988) presented reverse-time migration of crosswell seismic data by second-order finite differencing in space and time. Because of its strict requirements of fine spatial sampling, second-order finite differencing often is not sufficient for modeling surface seismic data that has a frequency band much lower than that of crosswell seismic data. The success of modeling high frequency crosswell seismic data depends on efficient implementation of high-order finite differencing, which requires much fewer spatial samples per wavelength for accurate numerical computation (Dablain, 1986). Gray and Lines (1992) introduced Kirchhoff depth migration of crosswell seismic data by two separate VSP migrations. However, their method is difficult to implement because it requires first decomposing the already complex wavefields into upgoing and downgoing reflections.

This paper first reviews modeling and migration, showing how they are interrelated. It then describes the application of fourth-order-in-time, tenth-order-in-space finite differencing to perform crosswell seismic modeling of the two-way acoustic wave equation, on velocity models that contain high-wavenumber velocity reflectors superimposed in a low-wavenumber smooth velocity background. Finally, it shows how reverse-time wavefield extrapolation coupled with the excitation-time imaging condition can be applied to perform migration on the scattered wavefields of crosswell seismic common-shot profiles. The modeling and migration are based on the geometry of a true field survey. At the end, the paper presents some suggestions to facilitate field data migration, which include removal of tube waves and wavefield separation.

REVERSE-TIME CROSSWELL DEPTH MIGRATION

The interrelation of modeling and migration

To describe modeling, let us consider the 2-D geological medium shown in Figure 1. It contains a point diffractor D in an arbitrary low-wavenumber velocity background. The recording geometry contains a source S located at one well and a series of receivers located at another well. During the modeling process, the direct wave emitted from the source S excites the diffractor D at a time equal to the minimum traveltime t_{SD} from the source S to the diffractor D, according to Fermat's principle. The diffractor D generates diffraction as rays DR that are recorded by the receivers. The diffraction wavefront expands from the diffractor. The direct wave SR does not pass through the diffractor D and thus does not bear information about the diffractor. The direct wave is muted before the data is input to the migration imaging process. Modeling by the finite-difference method represents the wave equation by finite-differencing. The low-wavenumber velocity background and the high-wavenumber velocity heterogeneity are represented as attributes assigned to the finite-difference grids. Each grid point is treated as a point diffractor (or secondary source). The strength of each secondary source is proportional to the reflectivity at that location. The recorded data are the history wavefields at the recording grid points (Mitchell, 1969; Alford et al. , 1974; Claerbout, 1976; McMechan 1985). During the process of modeling, the low-wavenumber velocity background governs the wave propagation, and the high-wavenumber velocity heterogeneity generates the diffractions. Crosswell seismic survey is usually conducted at a subsurface segment of the well that covers the target zone; thus, during the numerical modeling process, the absorbing boundary conditions of Clayton and Engquist (1977) are applied along the four sides of the grid to simulate a whole space for wave propagation.

Migration is the process that backprojects the recorded diffraction wavefields from the recording boundary into the low-wavenumber velocity background to locate the diffractors, which constitutes of the high-wavenumber velocity heterogeneity. What is needed as additional input is a low-wavenumber velocity background model that governs the wave propagation. Migration produces the image of high-wavenumber velocity heterogeneity, that is, the locations and strengths of the diffractors. Reverse-time depth migration projects the recorded diffraction wavefields back into the low-wavenumber velocity background by taking the recorded data as boundary values[2] of a finite-difference grid and running backward through time (McMechan, 1983). The diffraction wavefront focuses toward the location of the original diffractor. At time t_{SD}, all the energy that was diffracted at D will be focused at D. The value of the backpropagating wavefields at the particular grid point of D is extracted and then added as reflectivity into the image plane at the same spatial location (Chang and McMechan, 1986). As the wavefields continue to propagate backward in time, the focused energy at D defocuses and continues to backpropagate in the way each contribution originates. Each grid point is treated as a point diffractor and is imaged accordingly.

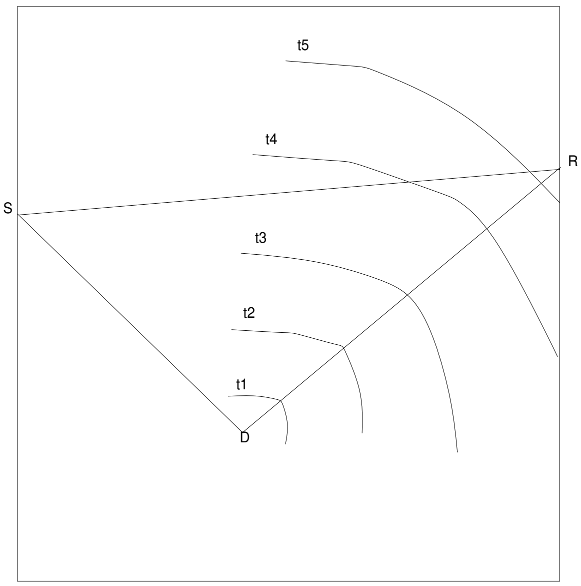

Figure 1: A crosswell recording geometry and demonstration of modeling and migration. During modeling, the diffraction wavefront expands from diffractor D. During reverse-time migration, the diffraction wavefront focuses toward diffractor D. mo2-Geometry [NR]

Crosswell seismic modeling

Figure 2 shows a vertically and horizontally variable but smooth background velocity model[3] whose velocity ranges from 4000 m/s to 5000 m/s. This model represents the results of transmission traveltime tomography. The crosswell survey with this velocity model is taken in a subsurface segment of the wells. The survey depth interval is 200 m. The two wells are separated by 100 m. The wavelet used in the finite-difference modeling is a Ricker wavelet whose frequency ranges from 200 Hz to 2000 Hz (Lazaratos et al., 1991), with the fundamental frequency being 1000 Hz. The dominant wavelength is 4 m; the smallest wavelength 2 m. The horizontal and vertical grid spacing is 0.5 m. Thus the spatial sampling interval is 4 points per wavelength for the smallest wavelength, which is a very coarse sampling interval. If

[2]For wave phenomena, boundary values are secondary sources, according to Huygens' wavefront construction principle (Mo, 1992).

[3]All the Raster figures in this paper are based on true relative amplitude, i. e., pclip=100.

second-order finite-differences were used, this spatial sampling would create severe grid dispersion. For the fourth-order-in-time, tenth-order-in-space finite differencing scheme employed in this paper, the numerical accuracy is very good.

Seismic modeling has been dominated by velocity models of velocity blocks with "knife-cut" sharp velocity contrast interfaces. These models do not correspond with the well logs and the field geology one sees. One never sees a well log with sharp contrast interfaces and never sees sharp contrast interfaces between different sedimentary rocks in field geology. Moreover, these models violate the theory of seismic data processing, which asserts that the low-wavenumber velocity, which is the smooth velocity background, governs the wave propagation, and the high-wavenumber velocity, which is the reflectivity, generates the diffractions. Inversion for velocity consists of two parts. The low-wavenumber velocity is inverted by transmission traveltime tomography, the high-wavenumber velocity by migration. What I did in this paper, I made the velocity model by superimposing high-wavenumber velocity contrast heterogeneity in a smooth background velocity model.

Imaging horizontal reflectors

On the above smooth background velocity model, I superimposed two horizontal reflectors. The reflector at a depth of 40 m is split at the horizontal position of 50 m vertically by 2 m, which is equal to half the dominant wavelength. The reflector at a depth of 160 m is split horizontally to generate a hole 22 m wide centered at the horizontal position of 50 m. The first Fresnel zone width at this depth relative to the source at a depth of 100 m on the left well is 22 m. I compute the Fresnel zone using Equation (8.2) (Yilmaz, 1987), which is valid for zero-offset surface surveys. The crosswell survey has a different geometry than a surface survey, and thus it should have a different formula to compute the Fresnel zone. However, I assume that the Fresnel zone width as computed by the formula valid for surface survey would not differ significantly from the true width of the crosswell Fresnel zone.

Figure 3(a) is the common-shot profile data generated by fourth-order-in-time, tenth-order-in-space finite-difference modeling with the source located at depth of 100 m in the left well and the receivers equally spaced at a depth interval of 0.5 m in the right well. Figure 3(b) shows the same common-shot profile data, but the direct wave has been muted because it does not help reflection imaging. The vertical faulting on the upper reflector and the horizontal faulting on the lower reflector have an effect of their reflection events. Figure 2 also shows the direct-wave traveltime contour map from the source computed by finite-difference method(Van Trier and Symes, 1990). It indicates the time that a diffractor is excited during modeling and also the time that the diffractor is imaged during migration wavefield backpropagation. With the recorded common-shot profile data as boundary conditions along the recording grid points, I run the two-way wave equation backward in time. Imaging is performed at each step of the wavefield extrapolation by extracting the values of the grid points that are imaged at that time as reflectivity and adding them into the image plane at

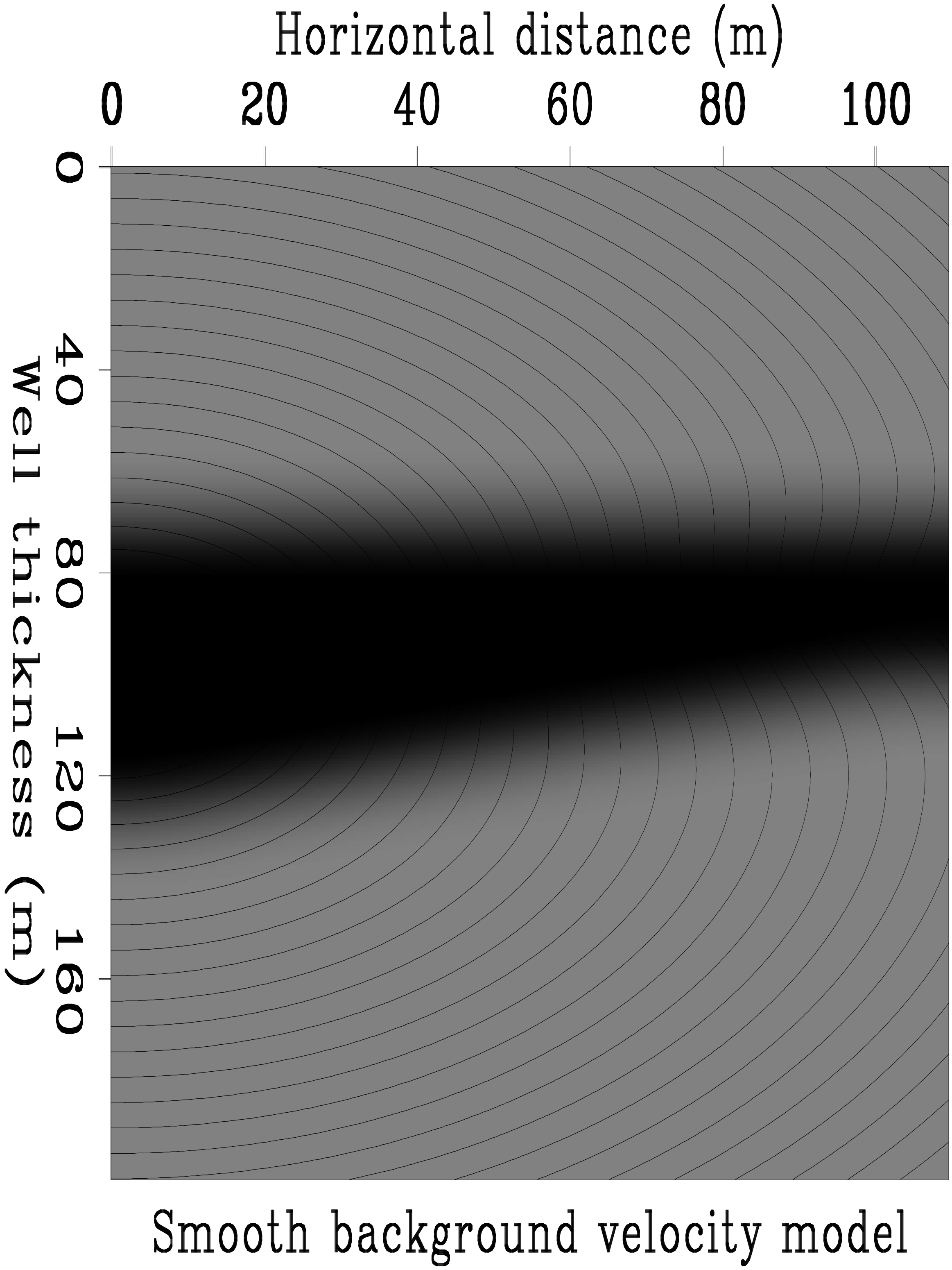

Figure 2: A smooth background velocity model, in which high-wavenumber velocity heterogeneity reflectors will be superimposed. Overlayed on this figure is the direct wave traveltime contour map from the source. mo2-BackTimemap [ER]

the same locations. The locus of all points that are imaged at a particular time step corresponds to the direct wave exciting wavefront from the source. The common-shot profile data that are input for migration processing are without divergence corrections because of the reversibility of modeling-migration conjugacy, which is explained in Appendix A. Using fourth-order-in-time, tenth-order-in-space finite differencing to solve the wave equation for migration wavefield backpropagation, I should gradually drop the order of central spatial finite differencing to the second-order near the recording boundary for the derivative perpendicular to the recording boundary, in order to avoid edge oscillation and ensure that the numerical solution conforms to physical wave phenomena. The coefficients of the second to tenth order of central finite differencing for the second derivative are given in the Appendix B. Figure 4 shows the reflectivity depth image between the two wells. The half wavelength of 2 m vertical faulting at a horizontal position of 50 m on the upper reflector can be clearly interpreted. The existence of the 22 m wide horizontal hole on the lower reflector can only be inferred because its dimension is equal to the corresponding 22 m wide first Fresnel zone.

There are some small artifacts in the image background. These artifacts can be diminished by using the redundancy stack of muti-shot migration images. It is remarkable that only one shot migration can image the reflectivity so well. In this migration scheme, one does not need to worry about the intrabed multiple reflections in the original data. The multiples are part of the total wavefields that propagate to their focuses during the migration wavefield backpropagation.

If there were diffractors with a depth very close to that of the source point, their diffraction response would be very close to that of the direct wave (Hu et al., 1988; Gray and Lines, 1992). Muting of direct waves would hurt such diffractions, and thus hurt the imaging of such diffractors. However, these diffractors can be effectively imaged by sources either above or below them.

Imaging dipping reflectors

On the above smooth background velocity model, I superimposed two dipping reflectors with depths of 40 m and 160 m at the left well. They both tilt 15-degree upward to produce opposite dip directions relative to the source. Figure 5(a) is the common-shot profile data generated by the same recording geometry as the above horizontal reflector case. Figure 5(b) shows data for the same common-shot profile after the direct wave has been muted. It is clear that the opposite dipping reflectors generate reflection events with different amounts of moveout. Figure 6 is the reflectivity depth image between the two wells. All parts of the upper reflector are imaged clearly, with the exception of a short segment near the right receiver well. This segment is not imaged because its reflection event is damaged by direct wave muting. The left part of the lower reflector is not imaged. Ray tracing indicates that its reflections do not propagate to the receivers in the right well.

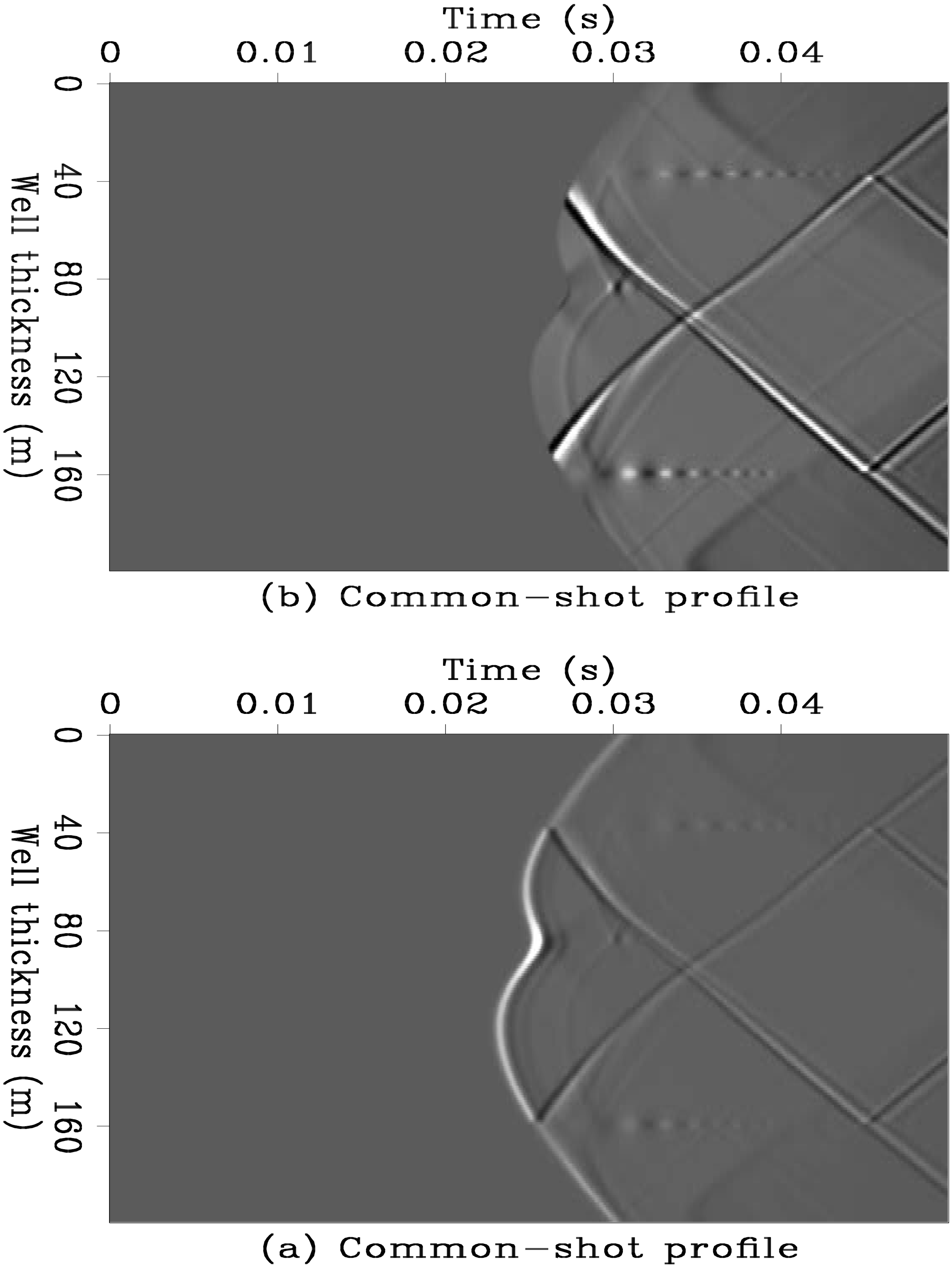

Figure 3: Crosswell common-shot profile, (a) the data without any processing, (b) after the direct wave has been muted. The vertical faulting on the upper reflector and the horizontal faulting on the lower reflector have an effect of their reflection events. $\boxed{\text{mo2-1DataH1H2}}$ [ER]

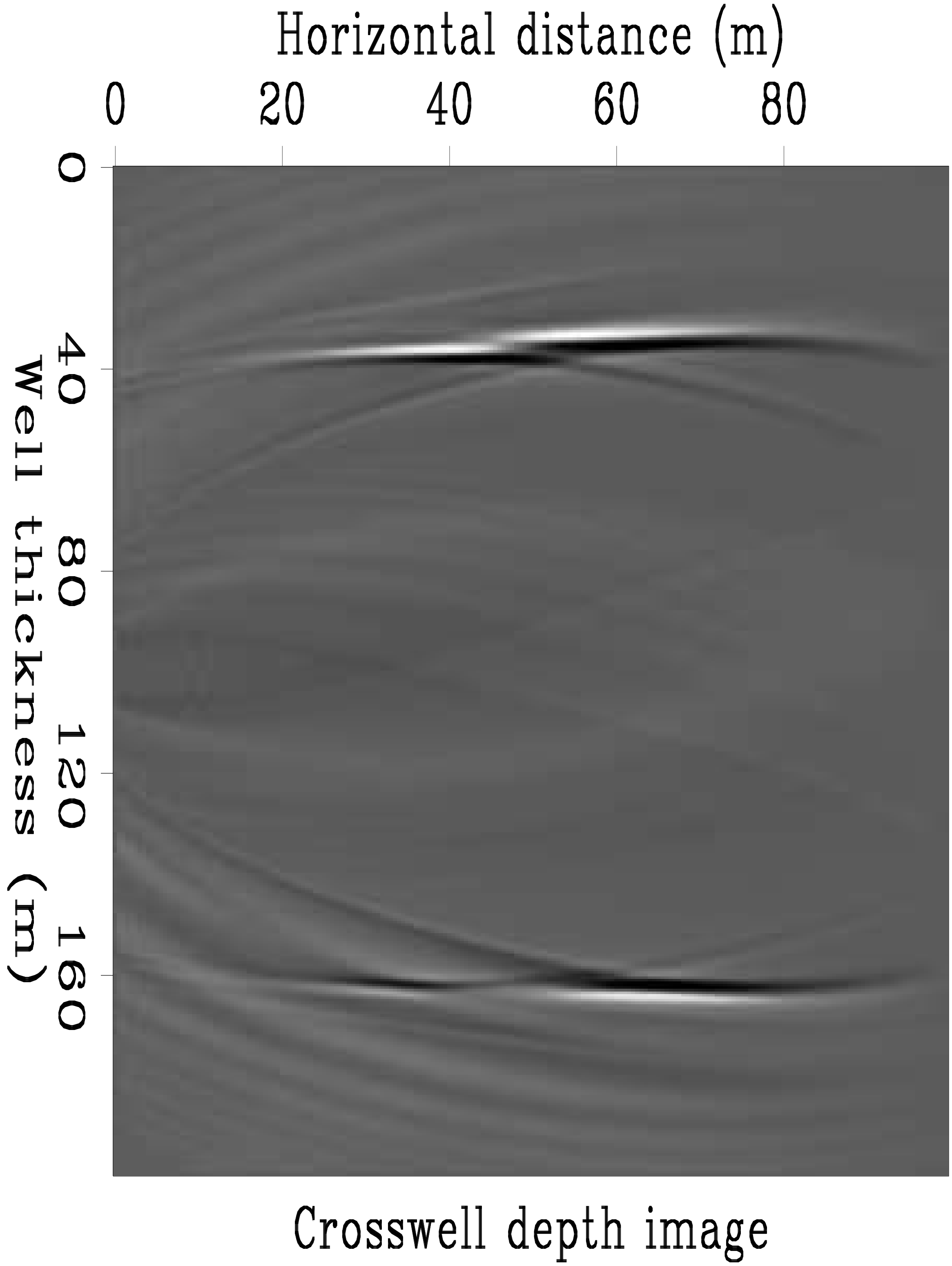

Figure 4: Crosswell depth image generated by migrating a common-shot profile. The half wavelength of 2 m vertical faulting on the upper reflector is clearly interpretable. The existence of the 22 m wide horizontal hole on the lower reflector can only be inferred because its dimension is equal to the corresponding 22 m wide first Fresnel zone. mo2-1Image.H [ER]

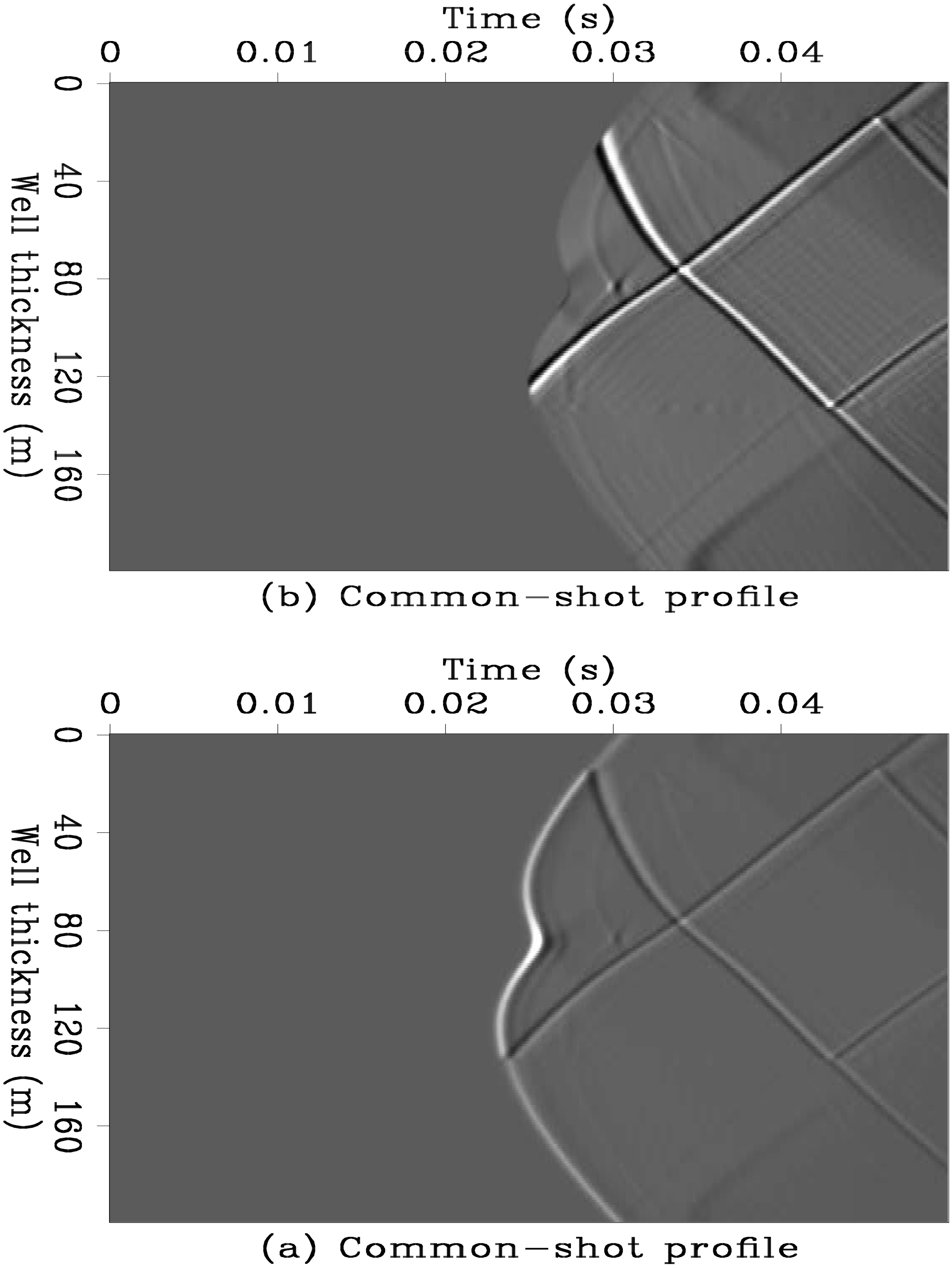

Figure 5: Crosswell common-shot profile, (a) the data without any processing, (b) after the direct wave has been muted. The opposite dipping reflectors generate reflection events with different amounts of moveout. $\boxed{\text{mo2-2DataH1H2}}$ [ER]

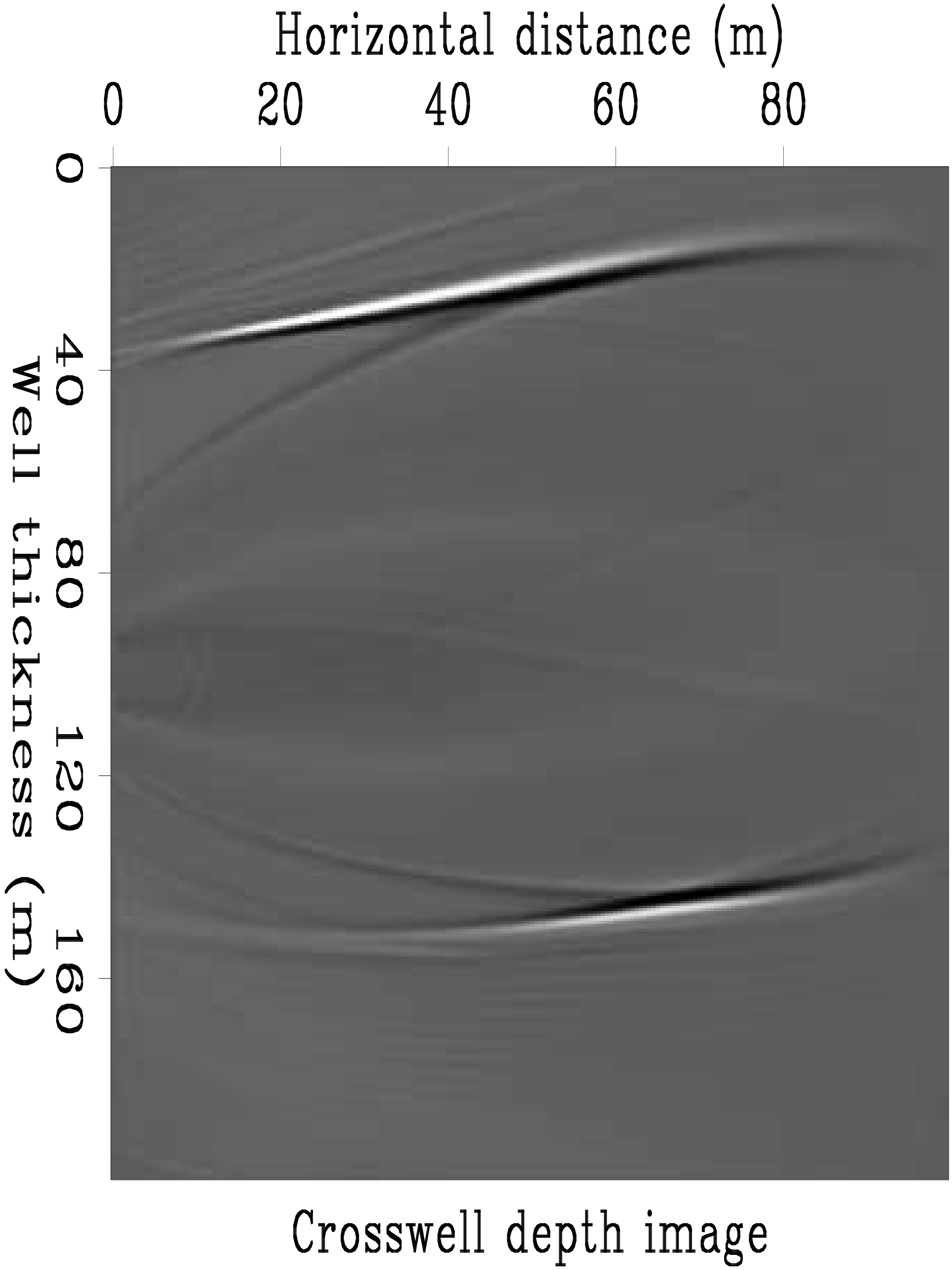

Figure 6: Crosswell depth image generated by migrating a common-shot profile. The two dipping reflectors have opposite dips relative to the source. The upper reflector is imaged clearly. The left part of the lower reflector is not imaged because its reflections do not propagate to the receivers well. mo2-2Image.H [ER]

DISCUSSION

Deviated well survey geometry can also be processed using the finite-difference method by applying the recorded wavefields as boundary conditions for the grid points corresponding to the receiver locations at the well.

The acoustic migration scheme presented in this paper can be readily extended to elastic reverse-time crosswell migration. In that case, we need to solve the elastic wave equation (Chang and McMechan, 1987).

In processing crosswell seismic data, a thorny problem is that of removing the aliased tube waves. I found two methods in the literature for removing aliased coherent noise such as tube waves. One method given by Zhang et al. (1992), first applies spatial interpolation and then does dip filtering to remove the aliased tube waves. The other scheme given by Turner (1990), applies notch filters directly in the $\tau - p$ domain of the original data to remove the aliased tube waves. After the aliased tube waves are removed, the data corresponding to the original receiver locations are again interpolated by the 2-D Fourier transform method, with the temporal and depth intervals chosen to satisfy the numerical grid dispersion relation. I assume that the reflection signals are well sampled in the field survey and that only tube waves are aliased.

Another problem is the handling of multi-component wavefields. The seismic source generates both P and S waves. If the field data is hydrophone data, it contains both P and S waves (Beydoun et al., 1989). This data can be dip filtered into P and S wave components. Then each component is processed independently as an acoustic wave. I assume that wave mode conversion is weak, so that the direct P wave excites P wave diffractions, and the direct S wave excites S wave diffractions. The other option is to transform the hydrophone data into a vector particle-displacement field (Cunha Filho, 1992) – vertical and horizontal components – and then feed the vector particle-displacement field data into an elastic migration scheme. If the field data are geophone vector particle-displacement multi-component data, then the data are directly fed into an elastic migration scheme to generate multi-component images.

CONCLUSIONS

Acoustic crosswell seismic modeling and migration has been successfully performed for a true field survey geometry by using high-order finite differencing. Vertical resolution up to a half wavelength and horizontal resolution as governed by the first Fresnel zone width have been realized.

ACKNOWLEDGMENTS

My thanks to the sponsors of SEP and its director, Professor Jon Claerbout, for their generous support. I am also grateful to John Etgen and Martin Karrenbach for discussions on finite-differences. In addition, I would like to thank the other members of the summer reservoir workshop group. Panel discussions at the group's seminar increased my understanding of crosswell seismic survey.

REFERENCES

Beydoun, W. B., and Mendes, M., 1989, Elastic ray-Born $l2$ migration/inversion: Geophys. J., **97**, 151–160.

Beydoun, W. B., Delvaux, J., Mendes, M., Noual, G., and Tarantola, A., 1989, Practical aspects of an elastic migration/inversion of crosshole data for reservoir characterization: A Paris basin example: Geophysics, **54**, 1587–1595.

Bregman, N. D., Bailey, R. C., and Chapman, C. H., 1989, Crosshole seismic tomography: Geophysics, **54**, 200–215.

Chang, W. F., and McMechan, G. A., 1986, Reverse-time migration of offset vertical seismic profiling data using the excitation-time imaging condition: Geophysics, **51**, 67–84.

Chang, W. F., and McMechan, G. A., 1987, Elastic reverse-time migration: Geophysics, **52**, 1365–1375.

Chen, S. T., Zimmerman, L. J., and Tugnait, J. K., 1990, Subsurface imaging using reversed vertical seismic profiling and crosshole tomographic methods: Geophysics, **55**, 1478–1487.

Claerbout, J. F., 1970, Coarse grid calculations of waves in inhomogeneous media with application to delineation of complicated seismic structure: Geophysics, **35**, 407–418.

Claerbout, J. F., 1976, Fundamentals of Geophysical Data Processing: McGraw-Hill.

Claerbout, J. F., 1985, Imaging the Earth's Interior: Blackwell Scientific.

Claerbout, J. F., 1991, Earth Soundings Analysis: Processing versus Inversion: Blackwell Scientific.

Clayton, R. W., and Engquist, B., 1977, Absorbing boundary conditions for acoustic and elastic wave equations: Bull. Seism .Soc. Am., **67**, 1529–1540.

Cunha Filho, C. A., 1992, Elastic modeling and migration in earth models: Ph. D. dissertation: Dept. of Geophysics, Stanford University.

Dablain, M., 1986, The application of high-order differencing to the scalar wave equation: Geophysics, **51**, 54–66.

Gray, S., and Lines, L., 1992, Cross-borehole tomographic migration: Amoco Research Center.

Harris, J. M., 1988, Cross-well seismic measurements in sedimentary rocks: 58th Ann. Internat. Mtg., Soc. Explor. Geophys., Expanded Abstracts, 147–150.

Hu, L. Z., McMechan, G. A., and Harris, J. M., 1988, Acoustic pre-stack migration of cross-hole data: Geophysics, **53**, 1015–1023.

Jacobs, A., 1982, The pre-stack migration of profiles: Ph. D. dissertation: Dept. of Geophysics, Stanford University.

Lazaratos, S. K., Rector, J. W., Harris, J. M., and Van Schaack, M., 1991, High-resolution imaging with cross-well reflection data: 61st Ann. Internat. Mtg., Soc. Explor. Geophys., Expanded Abstracts, 107–110.

Lines, L., 1991, Applications of tomography to borehole and reflection seismology: Geophysics: the leading edge of exploration, **10**, no. 7, 11–17.

Luo, Y., and Schuster, G. T., 1991, Wave-equation traveltime inversion: Geophysics, **56**, 645–653.

McMechan, G. A., 1983, Migration by extrapolation of time-dependent boundary values: Geophys. Prosp., **31**, 413–420.

McMechan, G. A., 1985, Synthetic finite-offset vertical seismic profiles for laterally varying media: Geophysics, **50**, 627–636.

McMechan, G. A., Harris, J. M., and Anderson, L. M., 1987, Cross-hole tomography for strongly variable media with application to scale model data: Bull. Seism. Soc. Am., **77**, 1945–1960.

Mo, L., 1992, Gaussian beam migration: SEP–**75**, 65–84.

Pratt, R. G., and Worthington, M. H., 1988, The application of diffraction tomography to cross-hole seismic data: Geophysics, **53**, 1284–1294.

Reshef, M., and Kosloff, D., 1986, Migration of common-shot gathers: Geophysics, **51**, 324–331.

Turner, G., 1990, Aliasing in the tau-p transform and the removal of spatially aliased coherent noise: Geophysics, **55**, 1496–1503.

Van Trier, J., and Symes, W. W., 1990, Upwind finite-difference calculation of traveltimes: SEP–**65**, 41–58.

Yilmaz, O., 1987, Seismic data processing: Soc. Expl. Geophys.

Zhang, L., Claerbout, J. F., and Ji, J., 1992, Seismic trace interpolation beyond spatial aliasing: SEP–**73**, 185–201.

Zhu, X., and McMechan, G. A., 1988, Acoustic modeling and migration of stacked cross-hole data: Geophysics, **53**, 492–500.

APPENDIX A

THE INPUT TO REVERSE-TIME MIGRATION

Reverse-time migration is the process that transfers recorded scattered data into the subsurface image by means of the two-way wave equation. The wave equation can be made to run both forward and backward in time. When the wave equation runs forward in time, it is a modeling process that transfers the subsurface reflectivity into scattered fields. When the wave equation runs backward in time, it is a migration imaging process that transfers the recorded scattered wavefields into the subsurface reflectivity image. The two processes are conjugate to each other (Claerbout, 1991), because the wave propagation wavefront is reversible. Thus the input to reverse-time migration is the recorded scattered data without divergence correction.

APPENDIX B

COEFFICIENTS OF 2ND- TO 10TH-ORDER CENTRAL DIFFERENCING FOR THE SECOND DERIVATIVE

In solving the wave equation by finite differencing, we should use central finite-difference schemes because the wave equation and physical wave phenomena are symmetric. And near a boundary with boundary conditions, we should gradually drop the order of finite differencing for the derivative perpendicular to the boundary.

The nth order central finite differencing for the second derivative is

$$\frac{\partial^2 \phi_i}{\partial x^2} = \frac{1}{\Delta x^2}\left[w_0\phi_i + \sum_{k=1}^{n} w_k(\phi_{i-k} + \phi_{i+k})\right] \tag{B-1}$$

For the 2nd order: w0=-2.; w1=1.

For the 4th order: w0=-5./2.; w1=4./3.; w2=-1./12.

For the 6th order: w0=-2.72222; w1=1.50000; w2=-0.15000; w3=1.11111E-02.

For the 8th order: w0=-2.84722; w1=1.60000; w2=-0.20000; w3=2.53968E-02; w4=-1.78571E-03.

For the 10th order[4]: w0=-2.92722; w1=1.66667; w2=-0.238095; w3=3.96825E-02; w4=-4.96031E-03; w5=3.17460E-04.

[4]Similar coefficients given in Dablain (1986) have been multiplied by a factor of 2. I do not know why.